Received: 6 December 2023 | Revised: 26 January 2024 | Accepted: 16 February 2024

DOI: 10.1002/biot.202300687

Biotechnology Journal

RESEARCH ARTICLE

Standardized approach for accurate and reliable model development of ion-exchange chromatography based on parameter-by-parameter method and consideration of extra-column effects

Yu-Cheng Chen[1] | Hui-Li Lu[2] | Rong-Zhu Wang[2] | Guo Sun[2] | Xue-Qin Zhang[2] | Jing-Qi Liang[2] | Alois Jungbauer[3] | Shan-Jing Yao[1] | Dong-Qiang Lin[1]

[1]Key Laboratory of Biomass Chemical Engineering of Ministry of Education, Zhejiang Key Laboratory of Smart Biomaterials, College of Chemical and Biological Engineering, Zhejiang University, Hangzhou, China

[2]Gmax Biopharm LLC., Hangzhou, Zhejiang, China

[3]Department of Biotechnology, University of Natural Resources and Life Sciences, Vienna, Austria

Correspondence
Dong-Qiang Lin, College of Chemical and Biological Engineering, Zhejiang University Hangzhou 310058, China.
Email: lindq@zju.edu.cn

Funding information
National Natural Science Foundation of China, Grant/Award Number: 22078286; Zhejiang Key Science and Technology Project, Grant/Award Number: 2023C03116; National Key R&D Program of China, Grant/Award Number: 2021YFE0113300; China Scholarship Council, Grant/Award Number: 202306320355; Zhejiang University Information Technology Center

Abstract

Developing an accurate and reliable model for chromatographic separation that meets regulatory requirements and ensures consistency in model development remains challenging. In order to address this challenge, a standardized approach was proposed in this study with ion-exchange chromatography (IEC). The approach includes the following steps: liquid flow identification, system and column-specific parameters determination and validation, multi-component system identification, protein amount validation, steric mass action parameters determination and evaluation, and validation of the calibrated model's generalization ability. The parameter-by-parameter (PbP) calibration method and the consideration of extra-column effects were integrated to enhance the accuracy of the developed models. The experiments designed for implementing the PbP method (five gradient experiments for model calibration and one stepwise experiment for model validation) not only streamline the experimental workload but also ensure the extrapolation abilities of the model. The effectiveness of the standardized approach is successfully validated through an application about the IEC separation of industrial antibody variants, and satisfactory results were observed with $R^2 \approx 0.9$ for the majority of calibration and validation experiments. The standardized approach proposed in this work contributes significantly to improve the accuracy and reliability of the developed IEC models. Models developed using this standardized approach are ready to be applied to a broader range of industrial separation systems, and are likely find further applications in model-assisted decision-making of process development.

KEYWORDS
antibody charge variant, extra-column effect, ion-exchange chromatography, model development, steric mass action model

Abbreviations: CST, continuously stirred tank; DPF, dispersed plug flow; EDM, equilibrium dispersive model; IEC, ion-exchange chromatography; IM, inverse method; LR1, first linear regression; LR2, second linear regression; PbP, parameter-by-parameter; SLA, simplified linear approximation; SMA, steric mass action.

1 | INTRODUCTION

Downstream processing involving multiple steps to isolate and purify the desired product from the cell culture medium, is pivotal for antibody and other protein drug production. In downstream processing of protein drugs ion-exchange chromatography (IEC) is widely used due to its high capacity, selectivity, and moderate prices.[1,2]

Achieving high-resolution IEC separation poses challenges, however, as individual components from upstream processes may have closely related elution behavior, which even may displace each other. A comprehensive understanding of these behavior is essential,[3] but it is cumbersome to obtain through experimental methods alone. In contrast, mechanistic models are extensively used in research related to IEC processes due to their robust interpretability and superior extrapolation abilities.[4–9] Regulatory authorities, such as those outlined in ICH-Q8(R2),[10] ICH-Q9,[11] and ICH-Q10,[12] emphasize that model-based process development contributes to a better understanding of complex elution behaviors. Beyond meeting ICH requirements, the industry is also moving toward implementing digital twins to operate process in a completely new environment.[13–16] The implementation holds promise in effectively reducing the time to market during the development of new biopharmaceuticals.[17] However, applying these models in industrial chromatography still presents several challenges, with one of the most significant being the development of accurate and reliable models.

In terms of model accuracy, it refers to the ability of the developed models to precisely depict the behavior of all components during the elution experiments. In other words, the developed mechanistic models serve as a complete mirror of the IEC process in the real world, forming a pair of digital twins. Figure 1 displays the potential errors during the model development.

(1) PDE errors: Mechanistic models commonly used in the modeling of IEC processes are primarily formulated as partial differential equations (PDEs). Developing PDEs that fully mirrors the IEC process is a highly challenging task. One crucial consideration is the bias-variance tradeoff, which implies a potential relationship between the complexity of PDEs and its bias-variance.[18] Reducing the PDE complexity may heighten bias but decrease variance. On the contrary, increasing the PDE complexity may reduce bias but increase variance (resulting in poor predictive ability) such as complex computational fluid dynamics (CFD) models.[19] But it requires detailed knowledge of the packing and flow path of the chromatography skid, making them computationally intensive.[20–22] It is essential to develop a simple yet efficient PDE to strike a balance in this trade-off. The most widely applied model in IEC is the steric mass action (SMA) model, comprising four parameters. It has been demonstrated to accurately predict the elution behavior of multi-component mixtures during IEC processes.[23] Therefore, the SMA model stands out as a sound choice. For industrial chromatography, solely modeling the chromatographic unit may not suffice to meet practical application demands. It is necessary to employ a series of PDEs to model the entire chromatography workstation, encompassing components such as pipelines, pumps, detectors, and more.

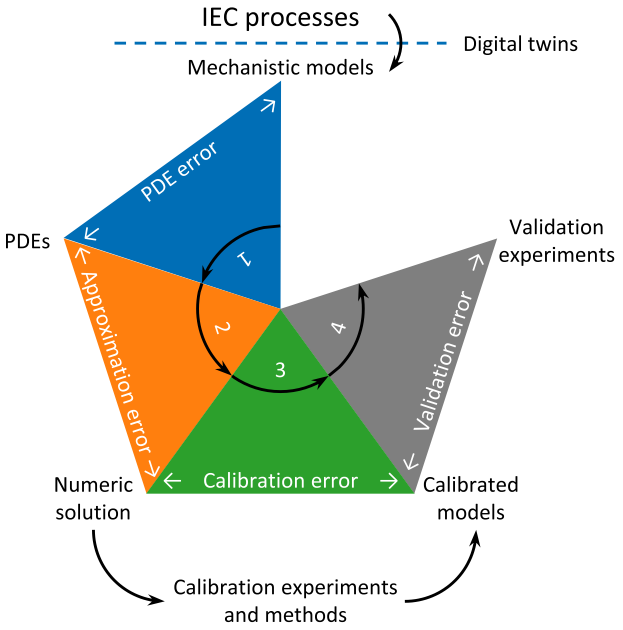

FIGURE 1 Four classes of errors in developing the mechanistic model for ion-exchange chromatography (IEC) processes.

This is essential due to the potential dominant impact of extra-column dispersion on resolution.[24,25]

(2) Approximation errors: Most of the chromatography PDEs lack analytical solutions. Obtaining numerical solutions for them through numerical methods introduces approximation errors. Discontinuous Galerkin finite element method has demonstrated outstanding accuracy and fast computational speed in solving stiff problems such as these chromatography PDEs.[26–28]

(3) Calibration errors: A model that accurately describes the IEC process cannot be directly obtained through experimental observations. Instead, we need to employ calibration experiments and methods to estimate the model parameters, leading to the introduction of calibration errors. There are three kinds of calibration experiments for the SMA model. First is the batch adsorption, which can be used to fit multiple adsorption isotherms under different salt concentrations. However, the generalization of the SMA model obtained from batch experiments to column experiments is questionable due to the neglect of column effects. Secondly, breakthrough experiments can be used to calibrate the SMA model. The third method is bind-and-elute experiments conducted under various operating conditions. The design of operating conditions will affect the calibration error. Regarding the parameter estimation methods for the SMA model through bind-and-elute experiments, the inverse method (IM) and the Yamamoto method[29,30] can be adopted. However, applying them to practical industrial applications has certain limitations. Specifically, the IM, reliant on reasonable initial guesses,[26] poses a challenge for novice modelers in determining suitable values. Additionally, there is an ongoing debate regarding whether the parameters obtained through the IM hold physical significance.[31,32] As for the Yamamoto method, it is only applicable to diluted conditions and not ideal for industrial chromatography with high protein loadings for ensuring productivity. To overcome the

limitations of these two methods, we proposed a more efficient approach, parameter-by-parameter (PbP) method.[33,34] This approach allows the users to obtain SMA parameters by determining retention of the components considered for modeling. Another advantage is its simplicity in calculations, involving only basic linear regressions and linear systems. These calculations can be readily calculated by novice modelers and easily implemented by Excel spreadsheets.[35] The concept of PbP calibration has been extended from the SMA model in the IEC field to the field of hydrophobic interaction chromatography.[36] Nevertheless, the PbP method has more stringent requirements for experimental design than other methods (such as gradient lengths and loading of elution experiments), posing a challenge for its applications. In the realm of industrial chromatography, it is essential to acknowledge that the absence of modeling extra-column dispersion could potentially introduce errors in the determination of retention times (which is particularly critical for the PbP method), thereby amplifying the calibration error.

(4) Validation error: The validation experiment is used to assess the generalization ability of the calibrated model. This validation error is unneglectable, but it should fall within an acceptable range. The design of validation experiments significantly influences the testing of this ability. Interpolative validation and extrapolative validation yield markedly different results. Validation through a well-designed and straightforward experiment would be optimal.

Above all, the errors in developing an IEC model result from four aspects. To minimize these errors and enhance the accuracy of the model, collaboration among researchers from various disciplines is essential. For instance, chemists can contribute by developing PDEs that more accurately describe the IEC process, while mathematicians can explore more efficient numerical methods. Those applying the models in industrial field should focus on the utilization of these models to reduce calibration and validation errors throughout the process.

In terms of model reliability, it relies on the establishment of such an accurate model mentioned above. Model reliability plays a crucial role in enhancing the dependability of model-assisted decision-making. Model-assisted decision-making has found widespread applications in the field of IEC, such as process optimization,[37] process characterization,[38] process scale-up,[25,39,40] and process control.[41] It is essential to consider the normativity and standardization of model development in IEC processes. A standardized and normative approach to model development ensures that the developed models meet regulatory standards and ensure product quality,[42] thereby enhancing the reliability of the models. In the era marked by a surge in mechanistic model research, ensuring the repeatability of model development becomes a crucial means of providing reliability to the models. This is particularly crucial for industrial applications. For instance, personnel in industry must ensure the accurate specification of models developed for different projects, adhering to uniform development standards. Moreover, adopting a standardized development approach will significantly optimize the workflow of the model development process and accelerate the speed of model development.

This study aims to present a standardized approach for developing an accurate and reliable model in IEC. In order to enhance the accuracy of the developed model, the proposed approach employs the PbP method as a calibration method (minimize the third-class calibration errors), elucidates the design of calibration and validation experiments (minimize the third-class and fourth-class errors), and considers the modeling of extra-column effect (minimize the first-class errors). In terms of model reliability, a standardized model development approach may contribute to its improvement. The approach includes the following steps: liquid flow identification, system and column-specific parameters determination and validation, multi-component system identification, protein amount validation, SMA parameters determination and evaluation, and validation of the calibrated model's generalization ability. Following sections will demonstrate its applicability through concrete examples about industrial antibody purification with an ÄKTA avant 25 system.

2 | MECHANISTIC MODELS

This section introduces several well-established models for various equipment in ÄKTA system, including the chromatographic column, extra-column equipment (e.g., tubes, valves, detectors, mixers and pumps), and the injection system. For detailed information on chromatographic models, readers are referred to relevant textbooks.[1,43]

2.1 | Models inside the column

The equilibrium dispersive model (EDM) is used as:

$$\frac{\partial c_i}{\partial t}(z,t) = -\frac{u_{\text{col}}}{\varepsilon_{\text{t}}}\frac{\partial c_i}{\partial z}(z,t) + D_{\text{app}}\frac{\partial^2 c_i}{\partial z^2}(z,t) - \frac{1-\varepsilon_{\text{t}}}{\varepsilon_{\text{t}}}\frac{\partial q_i}{\partial t}(z,t) \quad (1)$$

where c_i and q_i represent the liquid-phase and solid-phase concentration of protein i, respectively. z and t are the axial position and time, respectively. ε_{t} is the total porosity. D_{app} is the apparent axial dispersion coefficient. Superficial velocity u_{col} are calculated using volume flow $\dot{V}$, column length L, and total volume of a packed column V_{col}:

$$u_{\text{col}} = \frac{\dot{V}L}{V_{\text{col}}} \quad (2)$$

The model is completed with boundary conditions using the mobile-phase concentration of protein i at inlet $c_{\text{in},i}$:

$$D_{\text{app}}\frac{\partial c_i}{\partial z}(0,t) = \frac{u_{\text{col}}}{\varepsilon_{\text{t}}}\left[c_i(0,t) - c_{\text{in},i}(t)\right] \quad (3)$$

$$D_{\text{app}}\frac{\partial c_i}{\partial z}(L,t) = 0 \quad (4)$$

The kinetic SMA model with four parameters (characteristic charge ν, equilibrium coefficient k_{eq}, shielding factor σ, and kinetic coefficient

k_{kin}) and total ion-exchange capacity Λ is given by:

$$k_{kin,i} \cdot \frac{\partial q_i}{\partial t}(z,t) = k_{eq,i}\left[\Lambda - \sum_{j=1}^{n}(\nu_j + \sigma_j)\cdot q_j(z,t)\right]^{\nu_i} \cdot c_i(z,t) - q_i(z,t) \cdot c_s^{\nu_i}(z,t) \quad (5)$$

$$\frac{\partial q_s}{\partial t}(z,t) = -\sum_{j=1}^{n}\nu_j \cdot \frac{\partial q_j}{\partial t}(z,t) \quad (6)$$

where c_s and q_s represent the liquid-phase and solid-phase concentration of salt.

2.2 | Models outside the column

The dispersed plug flow (DPF) is used for tubing modeling:

$$\frac{\partial c_i}{\partial t}(z,t) = -u\frac{\partial c_i}{\partial z}(z,t) + D_{ax}\frac{\partial^2 c_i}{\partial z^2}(z,t) \quad (7)$$

where velocity u is calculated using the tube diameter d:

$$u = \frac{4\dot{V}}{\pi d^2} \quad (8)$$

and the axial dispersion coefficient D_{ax} is obtained by:

$$D_{ax} = 2ud \quad (9)$$

The boundary conditions, Equations (3) and (4), used in the column model are similarly implemented in the DPF model.

The ideal continuously stirred tank (CST) is employed for modeling of valves, mixers, and detectors using the hold-up volume V:

$$\frac{dc_i}{dt}(t) = \frac{\dot{V}}{V}\left[c_{in,i}(t) - c_i(t)\right] \quad (10)$$

2.3 | Model of injection system

The injection system can be characterized by a rectangular pulse:

$$c_{inj,i}(t_{inj}) = \begin{cases} c_{inj}x_i & 0 < t \le t_{inj} \\ 0 & t > t_{inj} \end{cases} \quad (11)$$

where $c_{inj,i}$ and x_i are the injection concentration and mole fraction of protein i, respectively. c_{inj} and t_{inj} represent the injection concentration and time, respectively.

The flow path equilibrated with the low-salt buffer before injection is applied as initial conditions for all equipment.

2.4 | Numerical solution

The column model and DPF model were spatially discretized using the discontinuous Galerkin finite element method. These models, along with the CST model, were solved using the solve_ivp solver in SciPy[44] with Python 3.10 and other packages (e.g., NumPy,[45] scikit-learn,[46] Pandas, and Matplotlib[47]).

2.5 | Parameter estimation

Table 1 enumerates all model parameters and the corresponding determination methods, categorized into three groups based on computability: known, experimentally determinable, and determinable via bind-and-elute experiments. The first two groups comprise system and column-specific parameters, while the SMA parameters in the third group are of particular importance and can be obtained using the PbP method. More details on the PbP method can be read in our previous publications.[33,34] In this work, a summary of the PbP method was provided:

(1) First linear regression (LR1) was applied to establish the relationship between the salt concentration at outlet at retention time of protein i, $c_{s,R,i}$, and the normalized gradient slope GH = $(1-\varepsilon_t)(c_{final} - c_{initial})/CV_G$ as:

$$\lg GH = m_{1,i}\lg c_{s,R,i} + n_{1,i} \quad (12)$$

where slopes $m_{1,i} = \nu_i + 1$ and intercepts $n_{1,i} = -\lg[k_{eq,i}(\nu_i+1)(\Lambda - a_i\bar{c}_{inj})^{\nu_i}]$. c_{final} and $c_{initial}$ are the salt concentration at inlet of gradient start and end, respectively. CV_G is elution volume with the unit of column volume (CV). m_1 can be employed to calculate ν as:

$$\nu_i = m_{1,i} - 1 \quad (13)$$

(2) Second linear regression (LR2) was used to establish the relationship between the term $10^{-n_{1,i}\cdot\nu_i^{-1}}(\nu_i+1)^{-\nu_i^{-1}}$ calculated by LR1 and loading conditions ($\bar{c}_{inj}$) as:

$$10^{-n_{1,i}\cdot\nu_i^{-1}}(\nu_i+1)^{-\nu_i^{-1}} = m_{2,i}\bar{c}_{inj} + n_{2,i} \quad (14)$$

where slopes $m_{2,i} = -k_{eq,i}^{\nu_i^{-1}}\cdot a_i$ and intercepts $n_{2,i} = k_{eq,i}^{\nu_i^{-1}}\cdot\Lambda$. Relative injection concentration $\bar{c}_{inj} = c_{inj}\cdot u\cdot t_{inj}/L$. n_2 can be utilized to estimate k_{eq} as:

$$k_{eq,i} = \left(\frac{n_{2,i}}{\Lambda}\right)^{\nu_i} \quad (15)$$

(3) Simplified linear approximation (SLA) for guessing the initial values of σ as:

$$\sigma_i = \frac{a_i}{k_{eq,i}}\frac{\bar{c}_{inj}}{c_{R,i}}\left(\frac{c_{s,R,i}}{\Lambda}\right)^{\nu_i} - \nu_i \quad (16)$$

where a_i is the nonlinear coefficient of protein i obtained by LR2, $c_{R,i}$ and $c_{s,R,i}$ are the mobile-phase concentration at outlet of protein i and salt at retention of protein i, respectively.

TABLE 1 Parameters of model and the corresponding methods for their determination.

Model	Symbol	Unit	Determination	Equation	Value
EDM	u_{col}	mm s^{-1}	Known	(2)	0.64
EDM	ε_t	–	Pulse injection	(18)	0.831
EDM	D_{app}	mm^2 s^{-1}	Pulse injection	(19)	0.0956
EDM	L	mm	Known	[-]	192
SMA	Λ	M	Acid–base-titration	(20)	0.61
SMA	ν	–	Bind-and-elute, LR1	(13)	[8.0, 8.3, 8.6]
SMA	k_{eq}	$\times 10^5$	Bind-and-elute, LR2	(15)	[4.4, 4.0, 3.2]
SMA	σ	–	Bind-and-elute, SLA + IM	(16)	[36.0, 67.1, 15.5]
SMA	k_{kin}	$\times 10^7$ sM^{ν}	Bind-and-elute, IM	(17)	[70.4, 27.0, 9.7]
DPF	u	mm s^{-1}	Known	(8)	[-]
DPF	D_{ax}	mm^2 s^{-1}	Known	(9)	[-]
DPF	L	mm	Known	[-]	[-]
DPF	d	mm	Known	[-]	[-]
CST	V	µL	Known or pulse injection	[-]	[-]

CST, continuously stirred tank; DPF, dispersed plug flow; EDM, equilibrium dispersive model; IM, inverse method; LR1, first linear regression; LR2, second linear regression; SLA, simplified linear approximation; SMA, steric mass action.

(4) Initial guesses of k_{kin} were determined by the heuristic algorithm. Then, the optimization problem was further solved with the objective function J as:

$$\min_{k_{kin},\sigma} J\left(c_{h,i}; k_{kin}, \sigma\right) := \min_{k_{kin},\sigma} \sum_{j=1}^{m} \sum_{i=1}^{n} \frac{\| c_i' - c_{h,i}\left(L, t; k_{kin,i}, \sigma_i\right) \|_{L^2}^2}{\| c_i' \|_{L^2}^2} \tag{17}$$

where m and n are the number of experiments and binding components, respectively. c_i' and $c_{h,i}$ are the measurement and numerical solution of mobile-phase concentration of protein i. $\| \cdot \|_{L^2}$ is L^2-norm.

3 | MATERIALS AND METHODS

3.1 | Resin, protein, and chemicals

The strong cation-exchange resin Eshmuno CPX (Merck KGaA, Darmstadt, Germany) was utilized. All column experiments were conducted using a column with a height of 192 mm and a volume of 15.1 mL in an ÄKTA avant 25 system (Cytiva, Uppsala, Sweden).

The antibodies of the immunoglobulin G type with a molecular weight of 148149 Da used in this study were obtained from Gmax Biopharm LLC., Hangzhou, China. The antibody was produced in Chinese hamster ovary cells, and subsequently purified using protein A affinity chromatography. The eluate from affinity chromatography was collected and the pH was adjusted to 7.0, and then carefully stored at a low temperature of −80°C to maintain stability until further use in this study.

Acetic acid sodium hydroxide and sodium chloride were supplied from Merck in Darmstadt, Germany. Morpholine ethyl sulfonic acid (MES) was purchased from Aladdin in Shanghai, China. All buffers were prepared using deionized water and filtered with a 0.2 µm sterile filter.

3.2 | Pulse injection experiments

ε_t and D_{app} can be determined by pulse injection experiments, involving the introduction of a nonbinding but pore-penetrating tracer, NaCl, onto the ÄKTA system. Using the injection of NaCl, ε_t was obtained by:

$$\varepsilon_t = \frac{V_{int} + V_{pore}}{V_{col}} = t_0 \cdot \frac{\dot{V}}{V_{col}} = \frac{V_R - V_{plant}}{V_{col}} \tag{18}$$

where V_{int} and V_{pore} represent the interstitial volume of the fluid phase and the volume of the particle pore system. t_0 is the column dead time. V_R and V_{plant} are the total dead time and the extra-column dead time of the system or plant.

Using the stage number of the cascade model developed by Martin and Synge,[48] D_{app} can be calculated by the first moment t_R and second moment σ_{casc} using the NaCl peak in pulse injection experiments as:

$$D_{app} = \frac{uL}{2\varepsilon_t N_{casc}} = \frac{uL}{2\varepsilon_t} \cdot \frac{\sigma_{casc}^2}{t_R^2} \tag{19}$$

Notably, this pulse injection approach was also employed for the assessment of the dead volume of other tubes and valves.

3.3 | Acid–base-titration experiments

Λ was determined by titration experiments. Initially, the packed column was equilibrated with deionized water and flushed with a solution

TABLE 2 Sample volumes, elution conditions, and R^2 of bind-and-elute experiments.

No.	Purpose	Loading [g L^{-1} column]	Injection volume (CV)	Elution condition	R^2		
					A1	A2	M
1	Calibration	10	0.52	Gradient 10 CV	0.71	0.88	0.91
2	Calibration	10	0.52	Gradient 15 CV	0.68	0.89	0.86
3	Calibration	10	0.52	Gradient 20 CV	0.70	0.90	0.92
4	Calibration	30	1.56	Gradient 10 CV	0.80	0.77	0.83
5	Calibration	40	2.08	Gradient 10 CV	0.86	0.65	0.73
6	Validation	10	0.52	Stepwise 5 CV	0.98	0.94	0.88

containing 0.5 M HCl. The system was then washed with deionized water again. Subsequently, a solution containing 0.1 M NaOH was introduced into the column until an observable increase in conductivity signal was detected at the column outlet. All experimental procedures were conducted in triplicate. Λ was calculated by:

$$\Lambda = c_{NaOH}\frac{V_{NaOH} - V_{plant} - V_{col}\cdot\varepsilon_t}{(1-\varepsilon_t)V_{col}} \quad (20)$$

where c_{NaOH} and V_{NaOH} are the concentration and volume of NaOH solution used for titration, respectively.

3.4 | Bind-and-elute experiments

The study involved six bind-and-elute experiments, consisting of five linear gradient elution experiments for model calibration and a stepwise elution experiment for model validation. These experiments were employed for the implementation of the PbP method. Our preliminary research has already elucidated how to design elution experiments to better utilize the PbP method.[33,34] The injection volumes of sample and elution conditions for bind-and-elute experiments are listed in Table 2.

The calibration experiment design adhered to the principle that three experiments with identical sample loading conditions but varying gradient lengths were used for LR1 calculation (e.g., experiments No. 1, 2, and 3 in Table 2), and three experiments with different sample loading conditions but identical gradient lengths were employed for LR2 calculation (e.g., experiments No. 1, 4, and 5 in Table 2). Consequently, a total of five experiments were utilized for model calibration. Linear gradient elution experiments needed complete elution of all components to be modeled within the linear gradient phase.

Stepwise elution, which differs from the gradient elution used in the calibration experiments, can be considered as the extreme case of infinite smoothness of the gradient and is suitable for testing the model's ability to predict beyond the calibration range.[42]

All elution experiments maintained consistent conditions, except for injection and elution conditions. The antibody sample was adjusted to pH 5.5 and injected at a concentration of 19.2 g L^{-1} by injection pump. A low-salt buffer with 50 mM acetate at pH 5.5 as well as a high-salt buffer of 50 mM acetate and 500 mM NaCl was prepared. The low-salt buffer was used for equilibration and washing of the chromatographic workstation. The mixture of these two buffers generated different Na^+ concentrations for the elution step, which was considered for modeling. A solution with 1 M NaOH were employed for column regeneration. Gradient elution experiments were executed with Na^+ concentrations ranging from 50 mM (0% high-salt buffer) to 300 mM (50% high-salt buffer). The elution peaks resulting from all experiments were collected in 2- or 3-mL fractions, in accordance with the injection volume of sample and elution conditions of each experiment. For the gradient elution, only the peak with a UV signal greater than 50 mAU at 280 nm was fractionated.

3.5 | Analytical methods

The protein sample and elution fractions were analyzed by weak cation-exchange HPLC with ProPacTM WCX-10 analytical column (Thermo, Waltham, USA) and Alliance e2695 HPLC system (Waters, Milford, USA). Equilibrium buffer was prepared using 20 mM MES buffer (pH 6.3), while elution buffer contained 0.5 M NaCl in 20 mM MES buffer (pH 6.3). The gradient was from 0% to 100% elution buffer in 50.0 min with flowrate of 0.5 mL min^{-1}. The protein response was detected using UV detector at 280 nm. The percentage of peak area was obtained via peak integration from HPLC chromatograms. Purity of the main variant was determined by dividing the main peak area by the total peak area of all variants.

4 | RESULTS AND DISCUSSION

The standardized approach for developing an accurate and reliable IEC model is shown in Figure 2. Validation of this approach was conducted through a case study addressing the separation of antibody variants.

4.1 | Identification of liquid flow

The flow path scheme (see Figure S1A) of ÄKTA avant 25 was available in ÄKTA manual with clear labeling. This scheme comprised three flows interconnected by the injection valve (V9-inj): injection flow, elution flow, and column flow. For modeling purposed, all equipment in the injection and column flows, as well as those in the elution flow that affect the system, were taken into account. This consideration was

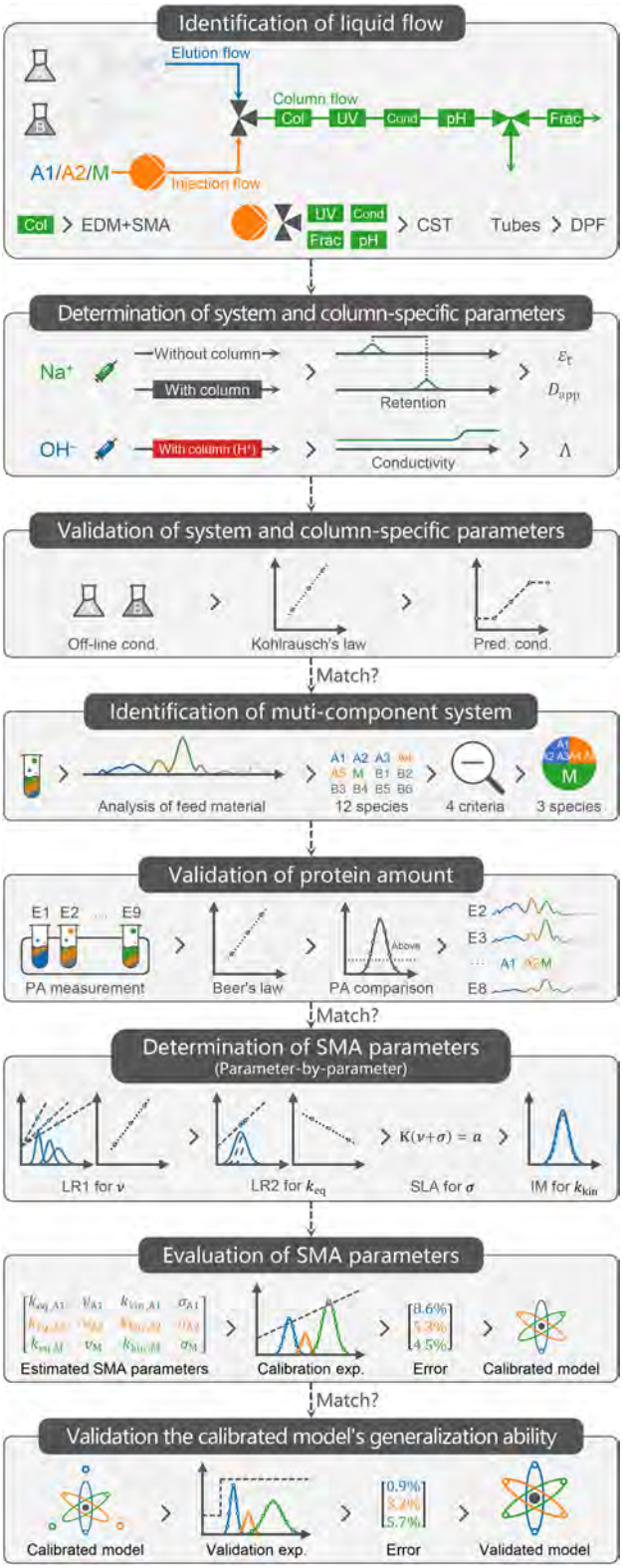

FIGURE 2 Standardized approach for accurate and reliable model development of ion exchange chromatography based on parameter-by-parameter method and consideration of extra-column effects.

based on the assumption that the fluid flow was homogeneous and well-mixed up to the restrictor (R9).

In the flows considered for modeling, all tubes were modeled using the DPF model with their lengths and diameters. The chromatographic column was modeled using a combination of the EDM and SMA models. The remaining equipment in the chromatography workstation were modeled with the CST model, which only requires knowledge of their volume. The model applied to each equipment is shown in Table 3 and Figure S1B (see the Supporting information).

4.2 | Determination of system and column-specific parameters

Table 1 includes the column-specific parameters that determined by pulse injection experiments and acid–base-titration experiments, including ε_t, D_{app}, and Λ. Table 3 outlines the system parameters of ÄKTA avant 25. The parameters that are not provided by the manufacturer were determined by pulse injection experiments.

4.3 | Validation of system and column-specific parameters

The system and column-specific parameters determined in the last section were validated by the conductivities of bind-and-elute experiments. For this purpose, the flow path was modified by employing the DPF model to describe the chromatographic column instead of the model combination of EMD and SMA models, with consideration of modeling of the salt species only.

In order to compare the experimentally measured conductivities with the salt concentrations predicted by models, the molar conductivities were required. It was calculated according to Kohlrausch's law for strong electrolytes under ideal dilution conditions on the basis of offline measurements of the conductivity of the solution.[1]

A good agreement between the predicted and experimental (dots) conductivities during the elution phase is observed in Figure 3, with $R^2 \approx 1.00$. It may due to the fact that we included the modeling of extra-column equipment.[24,25] However, slight differences were observed at retention times, where the simulated conductivities followed straight lines while the experimental values decreased, as shown in the bottom-right subplots of Figure 3. This difference might be caused by the high concentration of protein during elution, resulting in free sodium ions binding to the resin and thereby reducing the conductivity. An alternative explanation lies in the viscosity of solution. As the conductivity is a measure of ion mobility, a high concentration of protein induces lower ion mobility owing to the high solution viscosity.[1] Additionally, the top-left subplots of Figure 3 show sharp increases in the conductivity after injection, which might be due to protein binding to the resin releasing sodium ions from their original positions, thereby increasing the conductivity.

TABLE 3 Description of tubes, valves, pumps, detectors, and column in ÄKTA avant 25.

Label	Type	Diameter [mm]	Length [mm]	Volume [μL]	Model	From?
S1	Tube	1.60	700.0	1406.7	DPF	M
V9-IS	Valve	–	–	0.0	–	–
InS	Tube	1.60	220.0	442.1	DPF	M
P9-S	Pump	–	–	87.2	CST	E
1S1	Tube	0.75	340.0	150.1	DPF	M
1S2	Tube	0.75	340.0	150.1	DPF	M
2S	Tube	0.75	100.0	44.2	DPF	M
R9	Restrictor	–	–	87.2	CST	E
3S	Tube	0.75	485.0	214.2	DPF	M
3	Tube	0.75	280.0	123.6	DPF	M
M9	Mixer			1400.0	CST	M
4	Tube	0.75	400.0	176.6	DPF	M
V9-inj	Valve	–	–	87.2	CST	E
5	Tube	0.50	180.0	35.3	DPF	M
V9-C	Valve	–		87.2	CST	E
V9-C-in	–	–	–	1050.0	CST	M
Column	Column	10.0	192.0	15,072.0	EMD + SMA	E
V9-C-out	–	–	–	1050.0	CST	M
6	Tube	0.50	160.0	31.4	DPF	M
U9-D	Detector	–	–	2.0	CST	M
7	Tube	0.50	100.0	19.6	DPF	M
C9	Detector	–	–	22.0	CST	M
8	Tube	0.50	165.0	32.4	DPF	M
V9-pH	Detector	–	–	60.6	CST	M
1R	Tube	0.50	75.0	14.7	DPF	M
2R	Tube	0.50	75.0	14.7	DPF	M
9	Tube	0.50	215.0	42.2	DPF	M
V9-O	Valve	–	–	60.6	CST	M
Frac	Collector	0.50	1280.0	251.2	DPF	M

E: experimentally determinable, M: manufacturer available. CST, continuously stirred tank; DPF, dispersed plug flow; EDM, equilibrium dispersive model; SMA, steric mass action.

4.4 | Identification of the multi-component system

The weak cation-exchange HPLC chromatogram of the antibody sample in Figure 4 contains 12 species. Due to the complexity of modeling all of the variants, four criteria were developed to identify which species should be modeled in the multi-component system as:

(1) selecting only those variants adjacent to the main peak;

(2) choosing only those species with compositions exceeding a target specification;

(3) considering those peaks that could be reconstructed into a near-Gaussian shape in most fractions as one species[7];

(4) modeling together co-eluting species with near-identical retention times.

For the antibody showcase, three species, namely A1, A2, and M, comprising 86.3% of the feed material, were selected for modeling. This selection was based on criteria 1 and 2: retention times less than 30 min and area ratios above 10%. Three acidic variants were modeled as A1 (criterion 3), representing 22.3% (7.7% + 5.3% + 9.2%) of the feed material, and two acidic variants were modeled as A2 (criterion 4), representing 12.0% (8.8% + 3.2%) of the feed material. In particular, the biological activity and binding activity results (data not shown) demonstrated no significant difference in activity between main peak and its shoulder peak. Therefore, they were modeled as a single component, comprising 52.0% of the feed material. Finally, the basic variant on the right of the main variant was characterized as the amidated species at the C-terminal of the heavy chain, which is generally considered safe.[49]

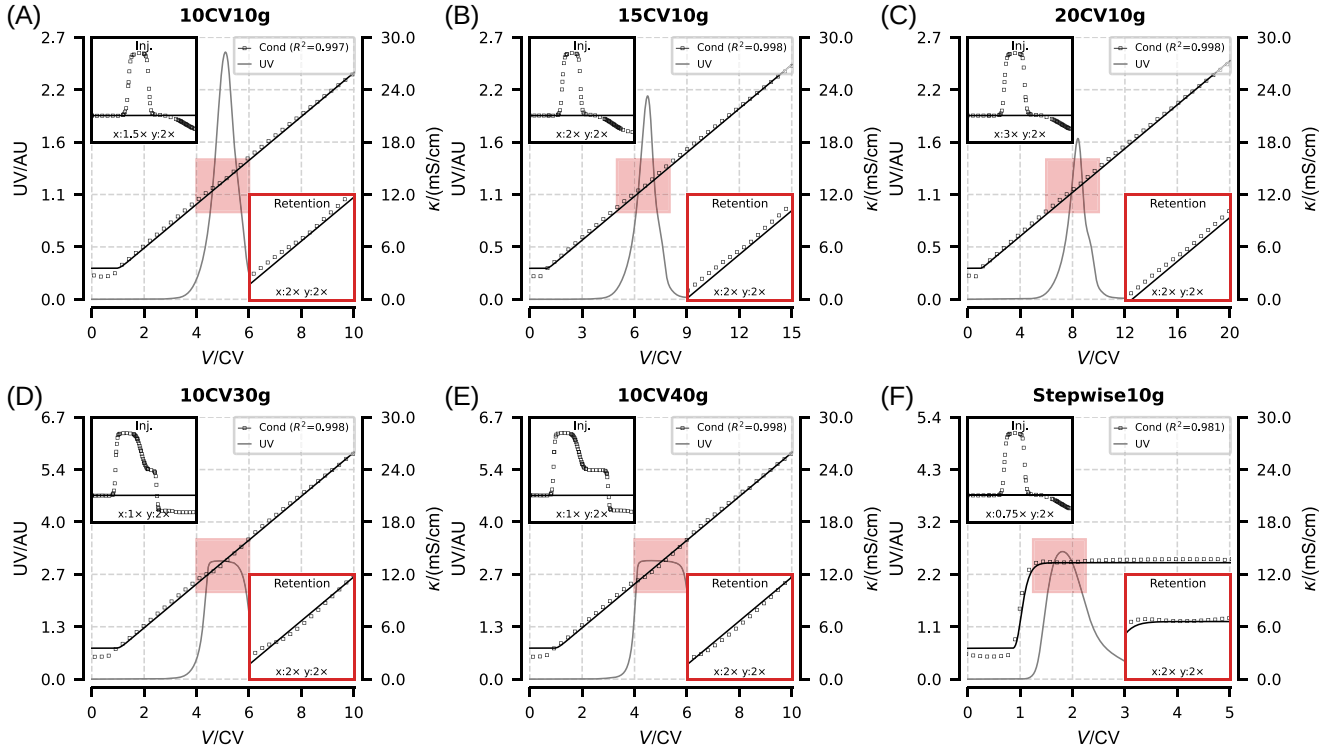

FIGURE 3 Conductivities of experiments (scatters) and model predictions (black lines). Grey lines: UV absorbance. Purposes: (A–E) calibration, (F) validation. Top-left: details during injection phase. Bottom-right: details of the red area at retention time.

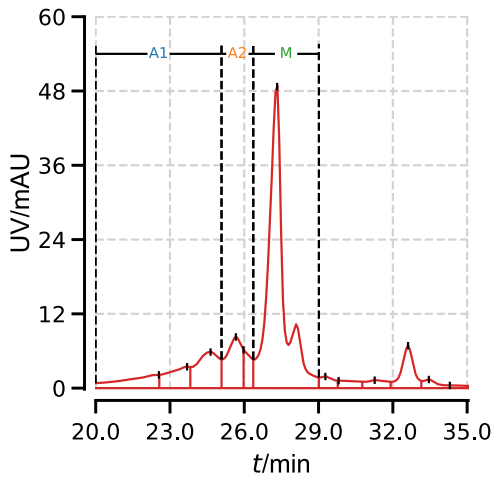

FIGURE 4 Weak cation-exchange HPLC chromatogram of feed material.

4.5 | Validation of protein amount

Elution peaks resulting from bind-and-elute experiments were collected, and the protein amount in each collection was measured and compared with UV absorbance obtained from the chromatographic system. The extinction coefficient, which converts mass concentration to UV absorbance, was calculated using Beer's law and considering the 2 mm path length of the UV sensor.[50] The average extinction coefficient of four experiments with a column loading of 10 g L^{-1} was 1.35 AU (g L^{-1})$^{-1}$ cm^{-1}, consistent with the reported value (1.42 AU (g L^{-1})$^{-1}$ cm^{-1} for antibodies).[51]

Using this extinction coefficient, the protein amount and UV absorbance curves are compared in Figure 5. It is noteworthy that the proportionate extinction coefficient obtained above is only valid within the linear range of UV and protein quantity conversion. The regions beyond the linear range, as shown in Figure 5D, E, lose the validity of this conversion due to excessively high concentrations, leading to lower R^2.

The comparison between UV and protein quantity plays a crucial role in the subsequent steps of this approach, particularly in the fraction analysis for bind-and-elute experiments. If issues arise during the validation of protein amount, hindering a satisfactory match, whether to proceed with further fraction analysis should be reconsidered. One of the major challenges in calibrating the SMA model by bind-and-elute experiments is the intensive analytical work, although this can be mitigated through alternative approaches such as peak deconvolution methods.[52]

Furthermore, this comparison allows us to identify which fractions significantly impact UV absorbance values and need to be analyzed. Employing this approach, we selected collections with a protein amount exceeding 0.7 g L^{-1} for analysis, while those not meeting this criterion were excluded. This decision also took into account the detection limit of the analytical equipment, below which the data would be unreliable, necessitating complex enrichment operations.

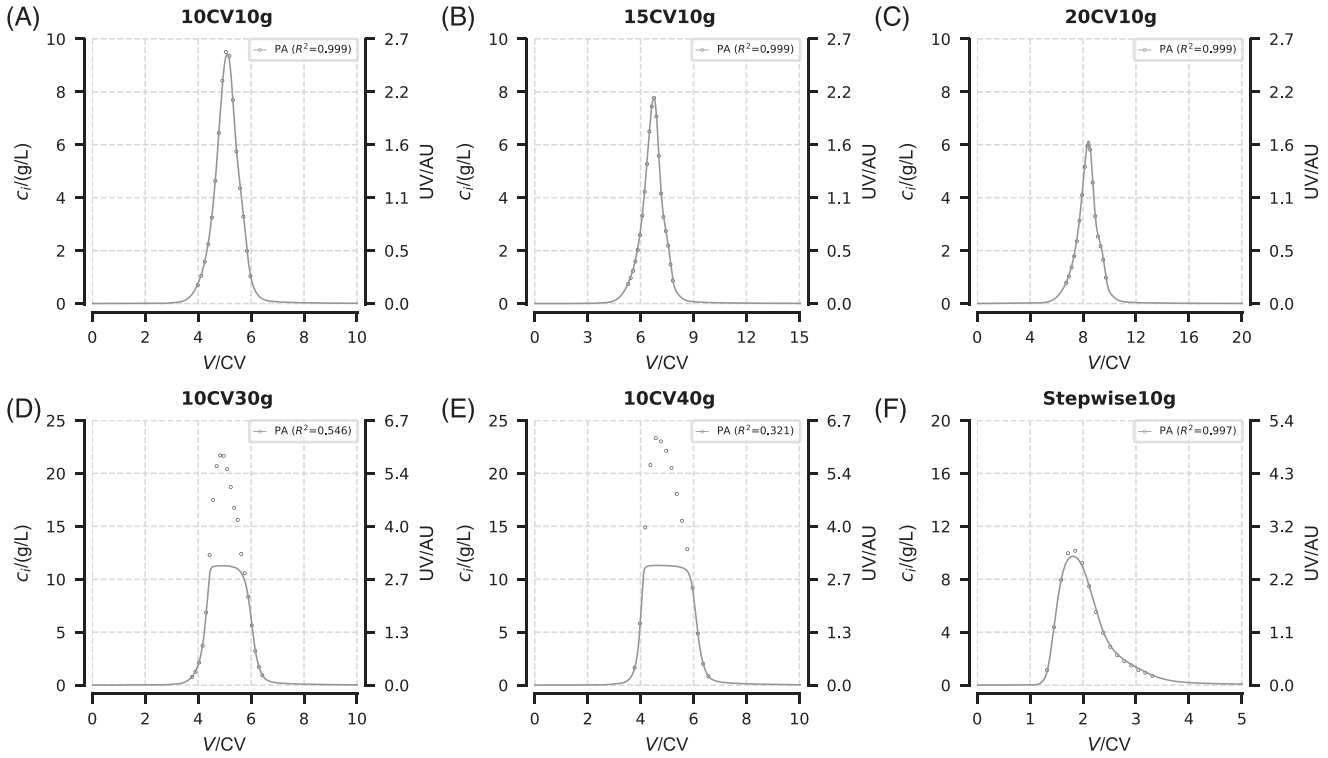

FIGURE 5 Protein amount of the collections (dots) and UV absorbance (lines). Purposes: (A–E) calibration, (F) validation.

4.6 | Determination of SMA parameters

The SMA model was calibrated by the PbP method as published in our previous papers.[33,34] Experiments No. 1, 2, and 3 in Table 2 are used for LR1 calculation with Equation (12), where GH is a known parameter. As for $c_{s,R,i}$, its determination involves the following steps: (1) identifying the retention time of the protein i through the first moment method and fraction analysis data; (2) locating the experimental value corresponding to this retention time from the outlet conductivity curve; (3) converting this experimental value into salt concentration using Kohlrausch's law. Experiments No. 1, 4, and 5 in Table 2 are used for LR2 calculation with Equation (14) where the left-hand-side term and $\bar{c}_{inj}$ can be obtained from LR1 and operating conditions, respectively.

Highly linear correlations for both LR1 and LR2 across all variants was found (Figure 6A, B), with R^2 approaching 1.00. ν and k_{eq} of each component were calculated by Equations (13) and (15), respectively, and are listed in Table 1. Notably, A1 and A2 had lower ν than M, consistent with previous report that antibody charge variants with higher ν had greater binding affinity to the cation-exchange resin and thereby eluted later.[7,26]

The SLA method yielded positive initial guesses of $\sigma_{A1} = 258.9$, $\sigma_{A2} = 359.8$, and $\sigma_M = 63.2$, consistent with the notion that σ represents the number of shielded sites on the adsorbent surface. Although some SMA models for antibody charge variants assume similar σ due to their identical molecular weights,[26,53] in this particular case, σ were significantly different. An interesting relationship between σ and the component's mole fraction x in the sample was found as $x_{A1}\sigma_{A1} \approx x_{A2}\sigma_{A2} \approx x_M\sigma_M$, indicating that the variant with a higher x has a smaller σ. This relationship can be rewritten as $x_{A1}(\nu_{A1} + \sigma_{A1}) \approx x_{A2}(\nu_{A2} + \sigma_{A2}) \approx x_M(\nu_M + \sigma_M)$ because ν were similar for all variants. The rewritten formula was likely to the SMA model's nonlinear term, $\sum_{j=1}^{n}(\nu_j + \sigma_j)q_j$, which represents the contribution of each component to SMA. Thus, the observation indicated that the different variants' σ can be distinct, but their contributions to SMA were equivalent. This relationship was also observed in previous investigation on σ for monomer-dimer mixtures of antibodies,[8,34] where $x_M(\nu_M + \sigma_M) \approx x_D(\nu_D + \sigma_D)$. For the system where the mole fraction of monomers was twice that of dimers,[8,34] the relationship can be rewritten as $\nu_D + \sigma_D \approx 2(\nu_M + \sigma_M)$, which is the basis of the self-association isotherm.[40,54–56]

However, the current interpretation was in conflict with the previously accepted explanation based on the same molecular weight. Evidently, this divergence aroused because the SLA method, which has an in-depth physical understanding of the SMA model, was employed to calculate σ. Conversely, the employment of a non-physically meaningful approach like the IM might not reveal this phenomenon.[35] Thus, the accuracy and interpretability of the SLA method for estimating σ were superior to those of the IM. Nevertheless, it remained uncertain whether the same molecular weight or equal contribution, is a better interpretation. Further research is necessary to address this question.

Subsequently, σ and k_{kin} were determined by solving the optimization problem defined in Equation (17). The results were $\sigma_{A1} = 36.0$, $\sigma_{A2} = 67.1$, and $\sigma_{Main} = 15.5$. All variants' σ were proportionately smaller than that of initial guesses. Notably, the algebraic relation $x_{A1}(\nu_{A1} + \sigma_{A1}) \approx x_{A2}(\nu_{A2} + \sigma_{A2}) \approx x_M(\nu_M + \sigma_M)$ was also observed.

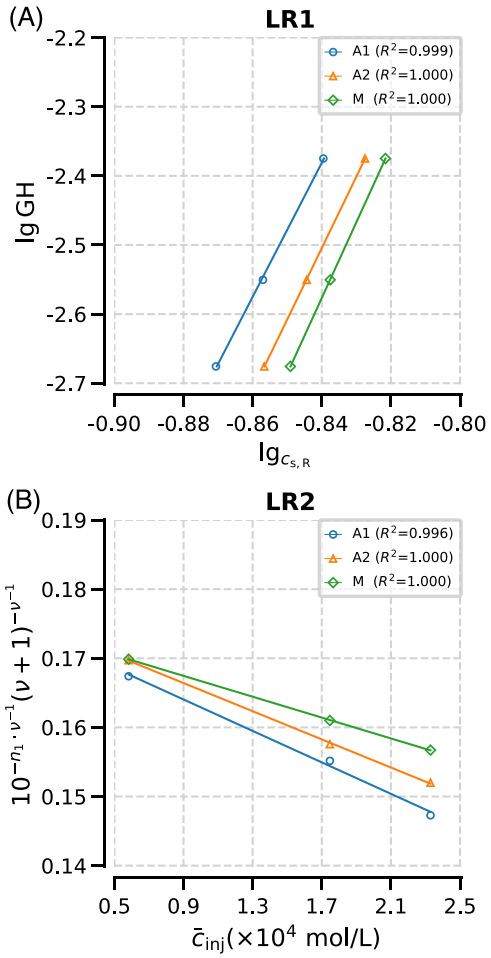

FIGURE 6 First linear regression (LR1) for ν and second linear regression (LR2) for k_{eq}.

The primary difference between the SMA and stoichiometric displacement models was the introduction of σ, similar to the divergence between the PbP and Yamamoto methods. Notably, σ accounted for the main reason why the SMA model can successfully generalize to the nonlinear adsorption region.[6,9] However, the accurate calculation of σ was a complex and challenging task, and various approaches have been explored in recent studies.[33,34,57,58]

4.7 | Evaluation of SMA parameters

Based on the estimated SMA parameters, the elution curves of calibration experiments with fraction analysis are compared in Figure 7A–E.

R^2 of five calibration experiments for variants A2 and M are close to 0.90, as listed in Table 2, indicating satisfactory agreement between the experimental and simulated results. In comparison, R^2 of A1 was lower, which might be due to grouping multiple acidic variants as a single component during component identification. Subsequently, we will assess the accuracy of the developed model in describing the IEC process in this case by analyzing peak retention times, heights, and conductivities.

Regarding the retention times, the experimental values matched well with model simulations for all variants in all experiments. This suggests that the PbP method derived from retention time can estimate the relationship between the SMA parameters and retention time.[33,34]

Regarding the peak heights, the simulated values of M in the experiments (10 g L^{-1} column loading) were slightly lower than those obtained experimentally. The simulated peak heights of all components in the experiments (30 and 40 g L^{-1} column loading in Figure 7D, E) were higher than the experiments, with lower R^2 compared to other experiments. This difference could be attributed to an increase in mass transfer resistance at high concentrations,[43] which violates the rapid equilibrium assumption of the EDM model. To account for this phenomenon, a more sophisticated mass transfer model may be needed.[9,59]

Regarding the conductivities, another difference between the models and experiments was observed after the sample injection, as shown in the top-left subplots of Figure 7. Compared to Figure 3 where the chromatographic column was modeled by the DPF model, Figure 7 partially predicts the increase in conductivities, but its magnitude was significantly lower than experiments. According to the mass conservation law, a decrease in conductivities must occur to compensate the increase. The compensation was observed at retention time, especially for high loadings (Figure 7E). By comparing conductivities in Figure 7E (SMA model) and Figure 3E (DPF model), it was concluded that the SMA model can describe the decrease in conductivities at retention time, which was mainly explained by Equation (6) in the SMA model.[23]

Based on a comprehensive analysis of peak retention times, heights, and conductivities, the model developed within this approach can be considered accurate in calibration experiments.

4.8 | Validation of the calibrated model's generalization ability

This section aimed to evaluate the calibrated model's generalization ability, also referred to extrapolation or prediction ability. Figure 7F presents the chromatogram with fraction analysis of the stepwise experiment ($R^2_{A1} = 0.98$, $R^2_{A2} = 0.94$, and $R^2_{M} = 0.88$). Notably, R^2 were higher than the calibration. This increase can be attributed to two factors. Firstly, the validation experiment contained denser fractions of A1, resulting in a better match of peak area for A1. Secondly, accurately predicting the conductivities through modeling of extra-column effects had a significant impact on the stepwise experiment.[25] These two reasons underscore the importance of designing the collection density and modeling extra-column effects based on the approach. Stepwise experiments were completely different from linear gradient elution experiments employed for calibration purposes. While efficiently reducing the number of experiments, they prove to be effective in evaluating the extrapolation capability and accuracy of models developed within this approach. This extrapolation-based validation approach is superior to the interpolation-based validation of linear gradient elution experiments.[58]

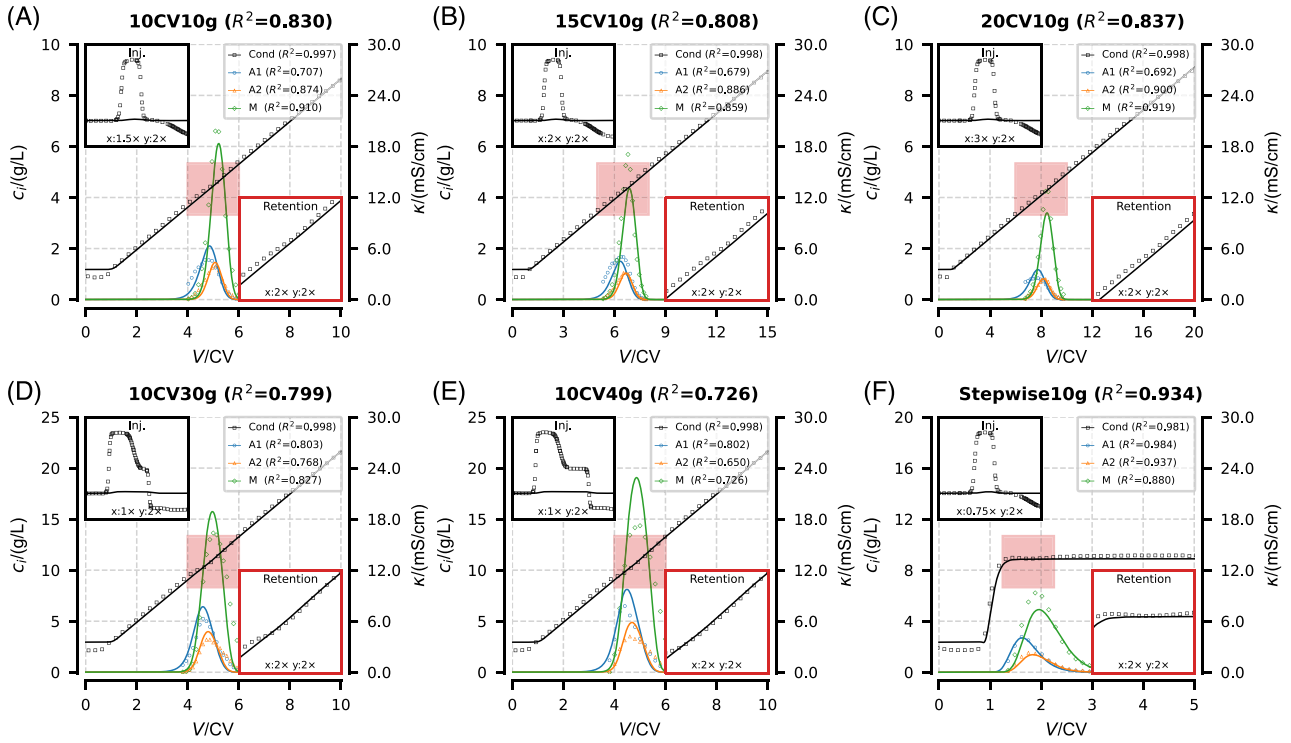

FIGURE 7 Chromatograms of experiments (scatters) and model simulations (colored lines). Black lines: conductivity curves predicted by models. Top-left: details during injection phase. Bottom-right: details of the red area at retention time.

5 | CONCLUSION

A standardized approach was proposed in this study to guide novice modelers to develop an accurate and reliable model for IEC processes. The proposed approach systematically introduced each aspect of standardized IEC modeling through a step-by-step approach. The effectiveness the developed approach is successfully validated through an application about the separation of antibody variants.

The standardized approach integrated the PbP calibration method to IEC modeling to enhance the accuracy of the developed models (minimize the third-class calibration and fourth-class validation errors). The experiments designed for implementing the PbP method (five experiments for model calibration and one for validation, respectively) not only streamline the experimental workload but also ensure the extrapolation abilities of the model. This accurate and reliable standardized approach to IEC modeling holds the potential to meet regulatory requirements and ensure consistency in model development. Models developed using this standardized approach are ready to be applied to a broader range of industrial separation systems, and will likely find further applications in model-assisted decision-making of process development.

AUTHOR CONTRIBUTIONS

Yu-cheng Chen: Conceptualization (lead), data curation (lead), formal analysis (lead), investigation (lead), methodology (lead), software (lead), validation (lead), visualization (lead), writing—original draft (lead). Hui-Li Lu: Conceptualization (lead), data curation (lead), investigation (lead), methodology (lead), validation (lead), writing—original draft (equal). Rong-Zhu Wang: Conceptualization (supporting), investigation (supporting), methodology (supporting), project administration (lead), resources (lead), supervision (supporting), writing—original draft (equal). Guo Sun: Investigation (supporting), methodology (supporting). Xue-Qin Zhang: Investigation (supporting), methodology (supporting). Jing-Qi Liang: Investigation (supporting), Methodology (supporting). Alois Jungbauer: Project administration (supporting), writing—review and editing (supporting). Shanjing Yao: Project administration (supporting), Resources (supporting), Supervision (supporting), Writing – review & editing (supporting). Dong-Qiang Lin: Conceptualization (lead), project administration (lead), resources (lead), supervision (lead), writing—review and editing (lead).

ACKNOWLEDGMENTS

This work was supported by the National Natural Science Foundation of China (22078286), Zhejiang Key Science and Technology Project (2023C03116), National Key R&D Program of China (2021YFE0113300), and China Scholarship Council (CSC, no. 202306320355). The authors also thank the Zhejiang University Information Technology Center for the cloud computing service.

CONFLICT OF INTEREST STATEMENT

The authors declare that they have no known competing financial interests or personal relationships that could have appeared to influence the work reported in this paper.

DATA AVAILABILITY STATEMENT

The data that support the findings of this study are available from the corresponding author upon reasonable request.

ORCID

Alois Jungbauer https://orcid.org/0000-0001-8182-7728
Shan-Jing Yao https://orcid.org/0000-0003-3199-3044
Dong-Qiang Lin https://orcid.org/0000-0002-0504-8391

REFERENCES

1. Carta, G., & Jungbauer, A. (2020). Introduction to protein chromatography. In *Protein Chromatography* (2rd ed., pp. 63–91). Wiley.
2. Qiao, L. Z., Du, Y. C., & Du, K. F. (2022). Grafting diethylaminoethyl dextran to macroporous cellulose microspheres: A protein anion exchanger of high capacity and fast uptake rate. *Separation and Purification Technology*, *297*(1), 121434. https://doi.org/10.1016/j.seppur.2022.121434
3. Vogg, S., Ulmer, N., Souquet, J., Broly, H., & Morbidelli, M. (2019). Experimental evaluation of the impact of intrinsic process parameters on the performance of a continuous chromatographic polishing unit (MCSGP). *Biotechnology Journal*, *14*(7). https://doi.org/10.1002/biot.201800732
4. Yoshimoto, N., Itoh, D., Isakari, Y., Podgornik, A., & Yamamoto, S. (2015). Salt tolerant chromatography provides salt tolerance and a better selectivity for protein monomer separations. *Biotechnology Journal*, *10*(12), 1929–1934. https://doi.org/10.1002/biot.201400550
5. Creasy, A., Barker, G., & Carta, G. (2017). Systematic interpolation method predicts protein chromatographic elution with salt gradients, pH gradients and combined salt/pH gradients. *Biotechnology Journal*, *12*(3). https://doi.org/10.1002/biot.201600636
6. Huuk, T. C., Hahn, T., Doninger, K., Griesbach, J., Hepbildikler, S., & Hubbuch, J. (2017). Modeling of complex antibody elution behavior under high protein load densities in ion exchange chromatography using an asymmetric activity coefficient. *Biotechnology Journal*, *12*(3), 1600336. https://doi.org/10.1002/biot.201600336
7. Kumar, V., & Rathore, A. S. (2017). Mechanistic modeling based PAT implementation for ion-exchange process chromatography of charge variants of monoclonal antibody products. *Biotechnology Journal*, *12*(9), 1700286. https://doi.org/10.1002/biot.201700286
8. Creasy, A., Reck, J., Pabst, T., Hunter, A., Barker, G., & Carta, G. (2019). Systematic interpolation method predicts antibody monomer-dimer separation by gradient elution chromatography at high protein loads. *Biotechnology Journal*, *14*(3), 1800132. https://doi.org/10.1002/biot.201800132
9. Morgenstern, J., Wang, G., Baumann, P., & Hubbuch, J. (2017). Model-based investigation on the mass transfer and adsorption mechanisms of mono-pegylated lysozyme in ion-exchange chromatography. *Biotechnology Journal*, *12*(9), 1700255. https://doi.org/10.1002/biot.201700255
10. ICH-Q8(R2). Pharmaceutical development. (2014).
11. ICH-Q9. Quality risk management. (2023).
12. ICH-Q10. Pharmaceutical quality system. (2014).
13. Narayanan, H., Sponchioni, M., & Morbidelli, M. (2022). Integration and digitalization in the manufacturing of therapeutic proteins. *Chemical Engineering Science*, *248*, 117159. https://doi.org/10.1016/j.ces.2021.117159
14. Sencar, J., Hammerschmidt, N., & Jungbauer, A. (2020). Modeling the residence time distribution of integrated continuous bioprocesses. *Biotechnology Journal*, *15*(8), 2000008. https://doi.org/10.1002/biot.202000008
15. Capito, F., Flato, H., Oeinck, V., Dierl, S., & Berg, A. (2022). Mimicking continuous capture chromatography for virus clearance using a single chromatography column model. *Biotechnology Journal*, *17*(5). https://doi.org/10.1002/biot.202100433
16. Chen, R., Chen, X. J., Shi, C., Jiao, B., Shi, Y., Yao, B., Lin, D. Q., Gong, W., & Hsu, S. (2022). Converting a mAb downstream process from batch to continuous using process modeling and process analytical technology. *Biotechnology Journal*, *17*(11). https://doi.org/10.1002/biot.202100351
17. Rish, A. J., Siddiquee, K., Huang, Z. R., Xu, J. L., Anderson, C. A., Borys, M. C., & Khetan, A. (2023). Strategies for controlling afucosylation in monoclonal antibodies during upstream manufacturing. *Biotechnology Journal*, *18*(7). https://doi.org/10.1002/biot.202200604
18. Bayer, B., Duerkop, M., Pörtner, R., & Möller, J. (2023). Comparison of mechanistic and hybrid modeling approaches for characterization of a CHO cultivation process: Requirements, pitfalls and solution paths. *Biotechnology Journal*, *18*(1). https://doi.org/10.1002/biot.202200381
19. Mayer, F., Cserjan-Puschmann, M., Haslinger, B., Shpylovyi, A., Sam, C., Soos, M., Hahn, R., & Striedner, G. (2023). Computational fluid dynamics simulation improves the design and characterization of a plug-flow-type scale-down reactor for microbial cultivation processes. *Biotechnology Journal*, *18*(1). https://doi.org/10.1002/biot.202200152
20. Jungreuthmayer, C., Steppert, P., Sekot, G., Zankel, A., Reingruber, H., Zanghellini, J., & Jungbauer, A. (2015). The 3D pore structure and fluid dynamics simulation of macroporous monoliths: High permeability due to alternating channel width. *Journal of Chromatography A*, *1425*, 141–149. https://doi.org/10.1016/j.chroma.2015.11.026
21. Schweiger, S., & Jungbauer, A. (2018). Scalability of pre-packed preparative chromatography columns with different diameters and lengths taking into account extra column effects. *Journal of Chromatography A*, *1537*, 66–74. https://doi.org/10.1016/j.chroma.2018.01.022
22. Iurashev, D., Schweiger, S., Jungbauer, A., & Zanghellini, J. (2019). Dissecting peak broadening in chromatography columns under non-binding conditions. *Journal of Chromatography A*, *1599*, 55–65. https://doi.org/10.1016/j.chroma.2019.03.065
23. Brooks, C. A., & Cramer, S. M. (1992). Steric mass-action ion exchange: Displacement profiles and induced salt gradients. *AIChE J.*, *38*(12), 1969–1978. https://doi.org/10.1002/aic.690381212
24. Kaltenbrunner, O., Jungbauer, A., & Yamamoto, S. (1997). Prediction of the preparative chromatography performance with a very small column. *Journal of Chromatography A*, *760*(1), 41–53. https://doi.org/10.1016/S0021-9673(96)00689-9
25. Saleh, D., Wang, G., Mueller, B., Rischawy, F., Kluters, S., Studts, J., & Hubbuch, J. (2021). Cross-scale quality assessment of a mechanistic cation exchange chromatography model. *Biotechnology Progress*, *37*(1), 13. https://doi.org/10.1002/btpr.3081
26. Meyer, K., Søes Ibsen, M., Vetter-Joss, L., Broberg Hansen, E., & Abildskov, J. (2023). Industrial ion-exchange chromatography development using discontinuous Galerkin methods coupled with forward sensitivity analysis. *Journal of Chromatography A*, *1689*, 463741. https://doi.org/10.1016/j.chroma.2022.463741
27. Breuer, J. M., Leweke, S., Schmölder, J., Gassner, G., & von Lieres, E. (2023). Spatial discontinuous Galerkin spectral element method for a family of chromatography models in CADET. *Computers & Chemical Engineering*, *177*, 108340. https://doi.org/10.1016/j.compchemeng.2023.108340
28. Andersson, D., Sjogren, R., & Corbett, B. (2023). Numerical simulation of the general rate model of chromatography using orthogonal collocation. *Computers & Chemical Engineering*, *170*, https://doi.org/10.1016/j.compchemeng.2022.108068
29. Yamamoto, S., Nakanishi, K., Matsuno, R., & Kamikubo, T. (1983). Ion exchange chromatography of proteins—prediction of elution curves and operating conditions. I. Theoretical considerations. *Biotechnology and Bioengineering*, *25*(6), 1465–1483. https://doi.org/10.1002/bit.260250605
30. Yamamoto, S., Nakanishi, K., Matsuno, R., & Kamikubo, T. (1983). Ion exchange chromatography of proteins-prediction of elution curves

and operating conditions. II. Experimental verification. *Biotechnology and Bioengineering*, *25*(5), 1373–1391. https://doi.org/10.1002/bit.260250516

31. Saleh, D., Wang, G., Muller, B., Rischawy, F., Kluters, S., Studts, J., & Hubbuch, J. (2020). Straightforward method for calibration of mechanistic cation exchange chromatography models for industrial applications. *Biotechnology Progress*, *36*(4), 12. https://doi.org/10.1002/btpr.2984
32. Rudt, M., Gillet, F., Heege, S., Hitzler, J., Kalbfuss, B., & Guelat, B. (2015). Combined Yamamoto approach for simultaneous estimation of adsorption isotherm and kinetic parameters in ion-exchange chromatography. *Journal of Chromatography A*, *1413*, 68–76. https://doi.org/10.1016/j.chroma.2015.08.025
33. Chen, Y.-C., Yao, S.-J., & Lin, D.-Q. (2022). Parameter-by-parameter method for steric mass action model of ion exchange chromatography: Theoretical considerations and experimental verification. *Journal of Chromatography A*, *1680*, 463418. https://doi.org/10.1016/j.chroma.2022.463418
34. Chen, Y.-C., Yao, S.-J., & Lin, D.-Q. (2023). Parameter-by-parameter method for steric mass action model of ion exchange chromatography: Simplified estimation for steric shielding factor. *Journal of Chromatography A*, *1687*, 463655. https://doi.org/10.1016/j.chroma.2022.463655
35. Chen, Y.-C., Chen, X.-Y., Lin, Z.-Y., Yao, S.-J., & Lin, D.-Q. (2023). Practical teaching of modeling tools for ion-exchange chromatography: A case study. *Journal of Chemical Education*, *100*(10), 3888–3896. https://doi.org/10.1021/acs.jchemed.3c00439
36. Yang, Y.-X., Chen, Y.-C., Yao, S.-J., & Lin, D.-Q. (2024). Parameter-by-parameter estimation method for adsorption isotherm in hydrophobic interaction chromatography. *Journal of Chromatography A*, *1716*, 464638. https://doi.org/10.1016/j.chroma.2024.464638
37. He, Q. L., von Lieres, E., Sun, Z. X., & Zhao, L. M. (2020). Model-based process design of a ternary protein separation using multi-step gradient ion-exchange SMB chromatography. *Computers & Chemical Engineering*, *138*, 106851. https://doi.org/10.1016/j.compchemeng.2020.106851
38. Saleh, D., Hess, R., Ahlers-Hesse, M., Beckert, N., Schonberger, M., Rischawy, F., Wang, G., Bauer, J., Blech, M., Kluters, S., Studts, J., & Hubbuch, J. (2020). Modeling the impact of amino acid substitution in a monoclonal antibody on cation exchange chromatography. *Biotechnology and Bioengineering*, *118*(8), 2923–2933. https://doi.org/10.1002/bit.27798
39. Keller, W. R., Evans, S. T., Ferreira, G., Robbins, D., & Cramer, S. M. (2022). Understanding the effects of system differences for parameter estimation and scale-up of high throughput chromatographic data. *Journal of Chromatography A*, *1661*, 462696. https://doi.org/10.1016/j.chroma.2021.462696
40. Koch, J., Scheps, D., Gunne, M., Boscheinen, O., & Frech, C. (2023). Mechanistic modeling of cation exchange chromatography scale-up considering packing inhomogeneities. *Journal of Separation Science*, *46*(9), 2300031. https://doi.org/10.1002/jssc.202300031
41. Bock, H. G., Cebulla, D. H., Kirches, C., & Potschka, A. (2021). Mixed-integer optimal control for multimodal chromatography. *Computers & Chemical Engineering*, *153*, 107435. https://doi.org/10.1016/j.compchemeng.2021.107435
42. Hess, R., Yun, D., Saleh, D., Briskot, T., Grosch, J.-H., Wang, G., Schwab, T., & Hubbuch, J. (2023). Standardized method for mechanistic modeling of multimodal anion exchange chromatography in flow through operation. *Journal of Chromatography A*, *1690*, 463789. https://doi.org/10.1016/j.chroma.2023.463789
43. Seidel-Morgenstern, A. (2020). Modeling of chromatographic processes. In H. Schmidt-Traub, M. Schulte, & A. Seidel-Morgenstern (Eds.), *Preparative chromatography* (3 ed., pp. 311–354). Wiley.
44. Virtanen, P., Gommers, R., Oliphant, T. E., Haberland, M., Reddy, T., Cournapeau, D., Burovski, E., Peterson, P., Weckesser, W., Bright, J., van der Walt, S. J., Brett, M., Wilson, J., Jarrod Millman, K., Mayorov, N., Nelson, A. R. J., Jones, E., Kern, R., Larson, E., … van Mulbregt, P. (2020). SciPy 1.0: Fundamental algorithms for scientific computing in Python. *Nature Methods*, *17*(3), 261–272. https://doi.org/10.1038/s41592-019-0686-2
45. van der Walt, S., Colbert, S. C., & Varoquaux, G. (2011). The NumPy array: A structure for efficient numerical computation. *Computing in Science & Engineering*, *13*(2), 22–30. https://doi.org/10.1109/MCSE.2011.37
46. Pedregosa, F., Varoquaux, G., Gramfort, A., Michel, V., Thirion, B., Grisel, O., Blondel, M., Müller, A., Nothman, J., Louppe, G., Prettenhofer, P., Weiss, R., Dubourg, V., Vanderplas, J., Passos, A., Cournapeau, D., Brucher, M., Perrot, M., & Duchesnay, É. (2011). Scikit-learn: Machine learning in Python. *Journal of Machine Learning Research*, *12*, 2825–2830. 10.48550/arXiv.1201.0490
47. Hunter, J. D. (2007). Matplotlib: A 2D graphics environment. *Computing in Science & Engineering*, *9*(3), 90–95. https://doi.org/10.1109/MCSE.2007.55
48. Martin, A. J. P., & Synge, R. L. M. (1941). A new form of chromatogram employing two liquid phases. *Biochemical Journal*, *35*, 1358–1368. https://doi.org/10.1042/bj0351358
49. Tsubaki, M., Terashima, I., Kamata, K., & Koga, A. (2013). C-terminal modification of monoclonal antibody drugs: Amidated species as a general product-related substance. *International Journal of Biological Macromolecules*, *52*, 139–147. https://doi.org/10.1016/j.ijbiomac.2012.09.016
50. Sejergaard, L., Karkov, H. S., Krarup, J. K., Hagel, A. B. B., & Cramer, S. M. (2014). Model-based process development for the purification of a modified human growth hormone using multimodal chromatography. *Biotechnology Progress*, *30*(5), 1057–1064. https://doi.org/10.1002/btpr.1923
51. Huuk, T. C., Hahn, T., Osberghaus, A., & Hubbuch, J. (2014). Model-based integrated optimization and evaluation of a multi-step ion exchange chromatography. *Separation and Purification Technology*, *136*, 207–222. https://doi.org/10.1016/j.seppur.2014.09.012
52. Briskot, T., Stuckler, F., Wittkopp, F., Williams, C., Yang, J., Konrad, S., Doninger, K., Griesbach, J., Bennecke, M., Hepbildikler, S., & Hubbuch, J. (2019). Prediction uncertainty assessment of chromatography models using Bayesian inference. *Journal of Chromatography A*, *1587*, 101–110. https://doi.org/10.1016/j.chroma.2018.11.076
53. Kumar, V., Leweke, S., von Lieres, E., & Rathore, A. S. (2015). Mechanistic modeling of ion-exchange process chromatography of charge variants of monoclonal antibody products. *Journal of Chromatography A*, *1426*, 140–153. https://doi.org/10.1016/j.chroma.2015.11.062
54. Seelinger, F., Wittkopp, F., von Hirschheydt, T., & Frech, C. (2022). Anti-Langmuir elution behavior of a bispecific monoclonal antibody in cation exchange chromatography: Mechanistic modeling using a pH-dependent self-association steric mass action isotherm. *Journal of Chromatography A*, *1689*, 463730. https://doi.org/10.1016/j.chroma.2022.463730
55. Mollerup, J. M., Hansen, T. B., Frederiksen, S. S., & Staby, A. (2010). Thermodynamic modeling of chromatographic separation. In E. Grushka, & N. Grinberg (Eds.), *Advances in chromatography* (Vol. 48, pp. 57–97). Taylor & Francis.
56. Koch, J., Scheps, D., Gunne, M., Boscheinen, O., Hafner, M., & Frech, C. (2022). Mechanistic modeling and simulation of a complex low and high loading elution behavior of a polypeptide in cation exchange chromatography. *Journal of Separation Science*, *45*(12), 2008–2023. https://doi.org/10.1002/jssc.202200098
57. Seelinger, F., Wittkopp, F., von Hirschheydt, T., Hafner, M., & Frech, C. (2022). Application of the Steric Mass Action formalism for modeling under high loading conditions: Part 1. Investigation of the influence of pH on the steric shielding factor. *Journal of Chromatography A*, *1676*, 463265. https://doi.org/10.1016/j.chroma.2022.463265

58. Osberghaus, A., Hepbildikler, S., Nath, S., Haindl, M., von Lieres, E., & Hubbuch, J. (2012). Determination of parameters for the steric mass action model—A comparison between two approaches. *Journal of Chromatography A*, *1233*, 54–65. https://doi.org/10.1016/j.chroma.2012.02.004
59. Lin, D.-Q., Zhang, Q.-L., & Yao, S.-J. (2021). Model-assisted approaches for continuous chromatography: Current situation and challenges. *Journal of Chromatography A*, *1637*, 461855. https://doi.org/10.1016/j.chroma.2020.461855

SUPPORTING INFORMATION

Additional supporting information can be found online in the Supporting Information section at the end of this article.

How to cite this article: Chen, Y.-C., Lu, H.-L., Wang, R.-Z., Sun, G., Zhang, X.-Q., Liang, J.-Q., Jungbauer, A., Yao, S.-J., & Lin, D.-Q. (2024). Standardized approach for accurate and reliable model development of ion-exchange chromatography based on parameter-by-parameter method and consideration of extra-column effects. *Biotechnology Journal*, *19*, e2300687. https://doi.org/10.1002/biot.202300687